Cell Calcium xxx (2013) xxx–xxx

Contents lists available at ScienceDirect

Cell Calcium

journal homepage: www.elsevier.com/locate/ceca

TRPM7 triggers Ca^{2+} sparks and invadosome formation in neuroblastoma cells

Daan Visser[a], Michiel Langeslag[b], Katarzyna M. Kedziora[a], Jeffrey Klarenbeek[a], Alwin Kamermans[a], F. David Horgen[c], Andrea Fleig[d], Frank N. van Leeuwen[e], Kees Jalink[a,*]

[a] Division of Cell Biology I, The Netherlands Cancer Institute, 1066 CX Amsterdam, The Netherlands
[b] Division of Physiology, Department of Physiology and Medical Physics, Medical University Innsbruck, A-6020 Innsbruck, Austria
[c] Laboratory of Marine Biological Chemistry, Department of Natural Sciences, Hawaii Pacific University, Kaneohe, HI 96744, USA
[d] Center for Biomedical Research, The Queen's Medical Center, Honolulu, HI 96813, USA
[e] Laboratory of Pediatric Oncology, Nijmegen Centre for Molecular Life Sciences, Radboud University, Nijmegen Medical Centre, 6500 HB Nijmegen, The Netherlands

ARTICLE INFO

Article history:
Received 8 July 2013
Received in revised form
27 September 2013
Accepted 28 September 2013
Available online xxx

Keywords:
Adhesion
Ca^{2+} imaging
Ca^{2+} signaling
Invadosome
TIRF microscopy
TRPM7

ABSTRACT

Cell migration depends on the dynamic formation and turnover of cell adhesions and is tightly controlled by actomyosin contractility and local Ca^{2+} signals. The divalent cation channel TRPM7 (Transient Receptor Potential cation channel, subfamily Melastatin, member 7) has recently received much attention as a regulator of cell adhesion, migration and (localized) Ca^{2+} signaling. Overexpression and knockdown of TRPM7 affects actomyosin contractility and the formation of cell adhesions such as invadosomes and focal adhesions, but the role of TRPM7-mediated Ca^{2+} signals herein is currently not understood. Using Total Internal Reflection Fluorescence (TIRF) Ca^{2+} fluorometry and a novel automated analysis routine we have addressed the role of Ca^{2+} in the control of invadosome dynamics in N1E-115 mouse neuroblastoma cells. We find that TRPM7 promotes the formation of highly repetitive and localized Ca^{2+} microdomains or "Ca^{2+} sparking hotspots" at the ventral plasma membrane. Ca^{2+} sparking appears strictly dependent on extracellular Ca^{2+} and is abolished by TRPM7 channel inhibitors such as waixenicin-A. TRPM7 inhibition also induces invadosome dissolution. However, invadosome formation is (functionally and spatially) dissociated from TRPM7-mediated Ca^{2+} sparks. Rather, our data indicate that TRPM7 affects actomyosin contractility and invadosome formation independent of Ca^{2+} influx.

1. Introduction

Cell migration is driven by the spatiotemporal regulation of cell adhesions and cytoskeletal contractility [1,2] and it is a prominent feature of cells throughout embryonic development as well as in adult life. Cell adhesions, such as focal complexes (FCs) and focal adhesions (FAs) link the extracellular matrix (ECM) to the actomyosin cytoskeleton and mediate traction at the leading edge of migrating cells, whereas their disassembly at the trailing edge allows cell detachment and net forward movement [3]. Local actomyosin contractility is a critical determinant of cell adhesion dynamics (i.e. formation, turnover and disassembly of adhesive structures) [1,4] and is under tight control of cellular signals such as the small GTPases Rho, Rac and Cdc42, [5,6] and Ca^{2+}. For example, it was recently proposed that localized Ca^{2+} signals (termed Ca^{2+} sparks or flickers) control lamellipodium protrusion and retraction and determine the direction of cell migration [7,8].

While much of what we know about dynamic control of cell adhesions has been learned from studies on FCs and FAs, more recently invadosome-type adhesions have become the subject of intense study. Invadosomes is a collective term that covers both podosomes in monocyte-derived cells and the closely related invadopodia in tumor cells [9]. Like FAs, these structures connect the cellular cytoskeleton to the ECM and sense mechanical forces [10], but they distinguish themselves by the ability to degrade ECM-components so as to facilitate cell invasion [9,11].

Abbreviations: 2-APB, 2-aminoethyl diphenylborinate; BK, bradykinin; ECM, extracellular matrix; FA, focal adhesion; FC, focal complex; TIRF, Total Internal Reflection Fluorescence (microscopy); TRPM7, Transient Receptor Potential cation channel, subfamily Melastatin, member 7.

* Corresponding author. Tel.: +31 020 512 1933; fax: +31 020 512 1944.
E-mail address: k.jalink@nki.nl (K. Jalink).

0143-4160/$ – see front matter © 2013 Elsevier Ltd. All rights reserved.
http://dx.doi.org/10.1016/j.ceca.2013.09.003

Invadosome biogenesis and turnover are modulated by cellular tension [4,12,13], mechanical cues [14,15] and receptor agonists [16–18], but the molecular mechanisms that coordinate invadosome dynamics are not well understood.

The role of (local) Ca^{2+} signals in controlling invadosome dynamics has remained largely understudied [19]. Invadosomes contain a variety of proteins that regulate actomyosin remodeling, many of which are Ca^{2+}-sensitive. In addition, several Ca^{2+}-permeable channels have been identified in invadosomes [19–21], including TRPV2 and TRPM7, two members of the Transient Receptor Potential (TRP) family of cation channels. TRP channels act as scaffolds for the assembly of large multiprotein complexes at the membrane and many of them are involved in sensory transduction [22,23]. TRPM7 (TRP subfamily Melastatin, member 7) is implicated in mechanotransduction [7,24,25] which is particularly intriguing as it is a bifunctional protein that consists of a non-selective divalent cation channel fused to an alpha-kinase [26–28]. Substrates for the TRPM7 kinase include annexin-1 [29] and myosin II isoforms [20,30]. Moreover, TRPM7 was demonstrated to regulate actomyosin contractility, cell adhesion and cell migration in a variety of cell types [7,20,31–34]. We, for example, previously demonstrated that in neuroblastoma cells (N1E-115) TRPM7 upregulation causes actomyosin relaxation, concomitant with formation of invadosomes, whereas in breast cancer cells (MDA-MB-231) knockdown of TRPM7 induced a contractile phenotype, which was accompanied by an increase in FA numbers [20,34]. Additionally, TRPM7 was shown to mediate localized Ca^{2+} influx in response to mechanical stress, which is thought to steer directional cell migration [7]. TRPM7 may therefore act as a mechanosensor that guides Ca^{2+}-mediated cytoskeletal rearrangements and cell adhesions. It is, however, unclear to what extent TRPM7-mediated Ca^{2+}-sparks drive local alterations in cell adhesion dynamics, as it has been difficult to dissociate the role of TRPM7 in ignition of Ca^{2+} signals from its function as a signaling scaffold and a kinase.

Given its enrichment at invadosomes and its contribution to Ca^{2+} spark formation, we hypothesized that TRPM7 mediates localized Ca^{2+} signaling events that modulate invadosome dynamics. To test this notion, we developed a sensitive assay to detect Ca^{2+} sparks at high spatiotemporal resolution and studied the dynamics of TRPM7-mediated invadosomes in N1E-115 cells.

2. Materials and methods

2.1. Materials and constructs

Ionomycin and bradykinin were from Calbiochem-Novabiochem (La Jolla, CA, USA). Fura Red-AM, Oregon Green 488 BAPTA-1-AM, EDTA-AM, Pluronic F-127 and Phalloidin-Alexa-586 were from Invitrogen (Eugene, OR, USA). Salts were from Merck (Darmstadt, Germany) and Dulbecco's MEM, fetal calf serum, penicillin and streptomycin were obtained from Gibco BRL-Invitrogen (Paisley, Scotland). The monoclonal vinculin antibody, Alexa488-conjugated secondary antibodies and 2-aminoethyl diphenylborinate (2-APB) were from Sigma–Aldrich (St. Louis, MO, USA). The TRPM7 antibody was from Alomone Labs (Jerusalem, Israel). Polyethylenimine (PEI, Linear, Cat# 23966-2) transfection reagent was from Polysciences Inc. (Warrington, USA). Lifeact-eGFP/dsRed and actin-mRFP were kind gifts of Dr. Michael Sixt (Institute of Science and Technology, Klosterneuburg, Austria) and prof. Dr. Rudolf E. Leube (Institute of Molecular and Cellular Anatomy, RWTH Aachen University, Aachen, Germany), respectively. Full length mouse TRPM7 cDNA, wild type (WT) cloned into LZRS-neo was previously described [20].

2.2. Isolation of waixenicin-A

Polyps of *Sarcothelia edmondsoni* were collected by hand at a depth of 1–3 m in Kailua Bay (Oahu, Hawaii). The freeze-dried polyps were ground by mortar and pestle and percolated exhaustively with hexane. The hexane extract was dried under vacuum and fractionated by first normal phase then reversed phase HPLC to give pure waixenicin-A. The compound identity was established by NMR (in d_6-benzene and d_4-methanol) and LCMS, in comparison to in-house reference data [43].

2.3. Cell culture and transfection

N1E-115 mouse neuroblastoma cells stably overexpressing TRPM7-HA and empty vector control were generated by retroviral transductions, as described elsewhere [20]. Cells were seeded on 24-mm glass-coverslips in 6-well plates in DMEM supplemented with 10% FCS (D10F) and antibiotics. Transfections were with PEI transfection reagent at 1 μg DNA per well per construct. The medium was refreshed 12–16 h after transfection.

2.4. Intracellular Ca^{2+} determinations

For pseudo-ratiometrical Ca^{2+} recordings, cells on glass coverslips were incubated for 30 min in a 200 μl volume of D10F containing Fura Red-AM (37 μM), Oregon Green 488 BAPTA-1-AM (8 μM) and Pluronic F-127 (0.1%), followed by further incubation in 2 ml HEPES-buffered saline (HBS), pH 7.3, for at least 15 min. HBS contained 140 mM NaCl, 5 mM KCl, 1 mM $MgCl_2$, 2 mM $CaCl_2$, 10 mM HEPES (pH 7.3) and 10 mM glucose. Coverslips were mounted on a Leica TCS SP5 confocal microscope and recordings were made at 37 °C in HBS. Excitation of Oregon Green-488 and Fura-Red was at 488 nm and fluorescence emission was detected at 500–550 nm and at >600 nm, respectively. All Ca^{2+} recordings are normalized by setting the response to ionomycin to 100%.

2.5. TIRF recording of Ca^{2+} spark activity

Cells were seeded on glass coverslips, transfected with actin-mRFP or Lifeact-dsRed where indicated, and cultured overnight in DMEM supplemented with 10% FCS and antibiotics. Cells were loaded simultaneously with the membrane-permeable fast Ca^{2+} indicator Oregon Green 488 BAPTA-1-AM (8 μM, Molecular Probes) and slow divalent chelator EDTA-AM (25 μM, Molecular Probes) according to the protocol detailed in the previous paragraph. Experiments were performed at 37 °C in HBS, pH 7.3.

Ca^{2+} sparks were imaged using a Leica AM TIRF MC microscope with a HCX PL APO 63x, 1.47 NA oil immersion lens. Excitation was at 488 nm and detection of fluorescence emission was by a QUAD/ET filter cube (Leica). Before each experiment, automatic laser alignment was carried out and TIRF penetration depth was set to 110 nm. Data were acquired for 100 s at 10 Hz frame rate and stored on disk.

TIRF time-series were subsequently processed with a custom-made analysis routine (macro) written for ImageJ 1.42 (NIH, USA) as described in detail in the text. The ImageJ macro is listed in Appendix A. Ca^{2+} spark activity over time was represented in heatmaps as detailed in the main text and in the legend to the figures. Briefly, individual calcium sparks were identified in time-lapse image series by thresholding and the resulting mask images were summed to create the single-image heatmap. Sites of recurrent (or prolonged) Ca^{2+} spark activity are termed Ca^{2+} hotspots. Each individual Ca^{2+} hotspot thus reflects the number of times the threshold (set to discriminate Ca^{2+} sparks from the background signal) was passed. For the 3-D representation of the heatmap, the ImageJ plugin 'Interactive 3D

surface plot' is used to depict Ca^{2+} spark density as the height of the plot (http://rsbweb.nih.gov/ij/plugins/surface-plot-3d.html). For detailed analyses automated Ca^{2+} spark detection was optionally fine-tuned by manual control of e.g. threshold levels.

2.6. Immunofluorescent stainings and gelatin degradation

Cells grown for 24 h on glass coverslips were fixed for 10 min at room temperature in phosphate-buffered saline (PBS) and 4% paraformaldehyde. Subsequently, cells were permeabilized with 0.1% triton X-100 in PBS. Cells were incubated with mouse anti-vinculin (1:200) or rabbit anti-TRPM7 (1:500) for minimally 60 min followed by Alexa-488-conjugated anti-mouse or anti-rabbit Ig (1:400), respectively. F-actin was visualized by Alexa-568-phalloidin (0.1 μg/100 μl). The cells were mounted in mowiol and imaged with a TCS-SP5 confocal microscope.

For matrix degradation assays, fluorescent gelatin-coated coverslips were prepared using 100 μg/ml gelatin-Oregon Green 488 (Invitrogen, Eugene, OR, USA). Poly-L-lysine coated coverslips were overlayed with a drop of gelatin-Oregon Green 488 for 30 min at room temperature, followed by cross-linking in ice-cold 0.5% gluteraldehyde. Using 5 mg/ml NaBH4, free gluteraldehyde reactive chains were quenched. Subsequently, coverslips were sterilized in 70% EtOH, washed with PBS and D10F, before N1E-115/TRPM7 cells (50,000) were seeded and incubated for 12–24 h at 37 °C and 5% CO_2. Finally, cells were processed as above to visualize the F-actin-dense core of invadosomes with Alexa-568-phalloidin (0.1 μg/100 μl). Typically, in this assay, focal sites of gelatin degradation appear as black spots as a result of secretion of metalloproteases at invadosomes.

2.7. Assaying cell shape and invadosomes

To study the effect of waixenicin-A on cell adhesion and spreading, cells (50,000/well) were seeded on 6-well culture dishes in D10F containing either vehicle (methanol) or waixenicin-A and assayed by time lapse microscopy using a Zeiss Axiovert or Leica Differential Interference Contrast (DIC) microscope for 2 h at 37 °C and 5% CO_2. Experiments were performed in 8-fold and cell adhesion and spreading were judged from stored data. Analysis was by detecting mean cell surface using ImageJ software.

To study the acute effects of treatment with waixenicin-A, cells were grown on glass coverslips for 24 h in D10F, mounted and transferred to a Leica TCS SP5 confocal microscope and maintained at 37 °C and 5% CO_2. Cells were imaged at two-minute intervals for up to 2 h. After a baseline recording (mock-treatment; methanol) of 15–30 min, waixenicin-A was added from a concentrated stock solution. The effect of treatment on number and turnover of invadosomes was assessed in cells expressing Lifeact-eGFP by counting. The effect of extracellular Ca^{2+} chelation by BAPTA on invadosomes was tracked in Lifeact-eGFP-positive cells for an extended period of time (>20 h). For these experiments, baseline recording (mock treatment) was 3 h and image interval was 3 min.

To determine whether chelation of intracellular Mg^{2+} by EDTA-AM treatment would affect invadosome characteristics (formation, architecture, dissolution etc.), Lifeact-eGFP cells were loaded as for Ca^{2+} spark experiments (see above) and cells were subsequently imaged at 3 min intervals for >20 h.

2.8. Statistics

The distribution of number of Ca^{2+} hotspots per cell appeared skewed to the left and was therefore analyzed by the non-parametric Mann–Whitney *U*-test. Continuous data that did approximate a Gaussian distribution were analyzed by the appropriate Student's *t*-test. Unpaired and paired categorical data were analyzed by the Fischer's exact test and the McNemar's test, respectively.

3. Results

3.1. TRPM7 and invadosomes

TRPM7 is expressed in most, if not all, cell types [26,27,35]. To directly test for a role of TRPM7 in the generation of Ca^{2+} sparks and their contribution to invadosome formation, we used a previously characterized variant of mouse N1E-115 neuroblastoma cells transduced with HA-tagged mouse TRPM7 to stably express TRPM7 up to ~3-fold of endogenous levels [20,36]. The vast majority of these N1E-115/TRPM7 cells contain invadosomes at the ventral plasma membrane ('central invadosomes'), underneath the nucleus (Fig. S1A, left panel). In a subset of the cells, we also observed prominent and very distinct invadosomes at the cell periphery ('peripheral invadosomes') that typically are larger in size than the central ones ([20] and Fig. S1A, right panel). Both types of invadosomes in N1E-115/TRPM7 cells are proteolytically active, as evidenced by the focal degradation of fluorescently labeled gelatin (Fig. S1B). As reported earlier, TRPM7 localizes to peripheral invadosomes ([20] and Fig. S1C and D), where it may affect invadosome formation, turnover or function, although this notion requires further evidence.

3.2. Ca^{2+} spark visualization

Local fast Ca^{2+} alterations such as Ca^{2+} sparks (for terminology see [37]) are usually hard to detect because they typically have a minor amplitude. Moreover, both free Ca^{2+} and dye-bound Ca^{2+} rapidly diffuse through the cytosol, quickly smoothing out any local elevations in free Ca^{2+}. One established method to detect Ca^{2+} sparks is to load cells with both a fast (binding rate of a few ms; [38]), low-affinity BAPTA-based Ca^{2+} indicator and with an excess of the slow (binding rate ~1 s), high-affinity Ca^{2+} chelator EGTA [39–41]. Thus, local high Ca^{2+} concentrations at entry sites rapidly light up the indicator, whereas spreading of the signal beyond a few micrometers is prevented by the slowly acting EGTA buffer. Furthermore, we used Total Internal Reflection Fluorescence (TIRF) microscopy to isolate local Ca^{2+} signals in the basal membrane from the bulk cytosolic signal at distances larger than ~200 nm from the coverslip.

We initially used membrane permeable AM-esters of the fast, low-affinity Ca^{2+} indicator Fluo-5F [Kd (Ca^{2+}) = 2.3 μM] and EGTA to load the cells, but failed to observe local or global fluctuations in fluorescence over time (data not shown). Fluo-5F, however, also failed to report the TRPM7-dependent sustained plateau phase of Ca^{2+} influx that typically follows the large Ca^{2+} peak from internal stores after stimulation with bradykinin (BK) in these cells ([36] and Fig. S2A). The sustained increases in $[Ca^{2+}]_i$ upon TRPM7 opening are small and hence likely below the detection limit of Fluo-5F. In the next experiments we therefore used the high-affinity Ca^{2+} indicator Oregon Green 488 BAPTA-1-AM which we used to study TRPM7-mediated Ca^{2+} influx in our previous study ([36] and Fig. S2B). Again, however, only very minor fluorescence fluctuations were observed in these TIRF time-lapses.

The activity of TRPM7 channels depends strongly on $[Mg^{2+}]_i$ [27] and lowering intracellular free Mg^{2+} by loading cells with the divalent chelator EDTA-AM augments both TRPM7 currents as detected by perforated patch clamp and Ca^{2+} influx as recorded by Ca^{2+} fluorometry in intact cells [36]. Strikingly, when we used EDTA-AM instead of EGTA-AM we readily observed Ca^{2+} sparks as small, localized and short-lived changes in fluorescence intensity in a large fraction of the cells (Video 1). We therefore adopted the latter conditions for the remainder of our experiments.

Please cite this article in press as: D. Visser, et al., TRPM7 triggers Ca^{2+} sparks and invadosome formation in neuroblastoma cells, Cell Calcium (2013), http://dx.doi.org/10.1016/j.ceca.2013.09.003

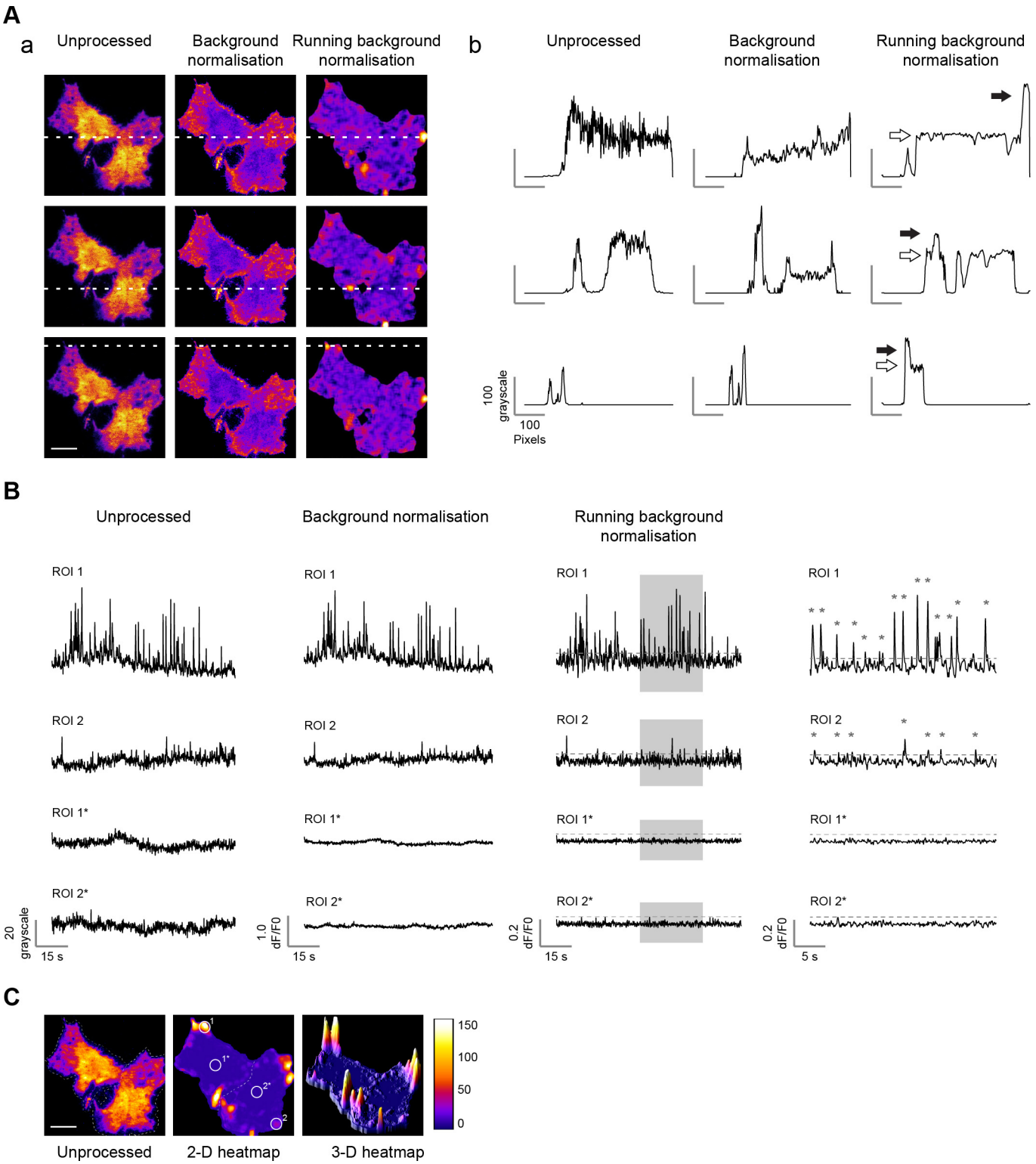

Fig. 1. EDTA-AM pretreatment unveils Ca^{2+} sparks in N1E-115/TRPM7 cells. (A) N1E-115/TRPM7 cells loaded with Oregon Green 488 BAPTA-1-AM and EDTA-AM were imaged for 100 s at 10 Hz frame rate by TIRF microscopy. (a) Left column: three examples of unprocessed images; middle column, images corrected by subtraction of a static background (i.e. the minimum intensity of the entire time-series); right column, images processed by the running background correction as detailed in the text. Note the normalization of cellular fluorescence signal and the much improved visualization of Ca^{2+} sparks in this column. (b) Intensity profiles taken along the dashed lines in each of the panels in a. Note that the uneven fluorescence present in the unprocessed images is effectively normalized by the running background correction (open arrows) enabling clear detection of Ca^{2+} sparks (closed arrows). (B) Representative Ca^{2+} traces for two ROIs (see C) with Ca^{2+} spark activity and two corresponding background (*) ROIs. Left column: in unprocessed traces Ca^{2+} sparks appear on a noisy background that shows local slow fluctuations (compare e.g. ROI-1 and ROI-2). High-amplitude Ca^{2+} sparks in ROI-1 can be easily thresholded but low-amplitude signals in ROI-2 are buried in background. The running background correction (column 3) but not the static correction (column 2) eliminates the fluctuations sufficiently to allow discrimination of low-amplitude signals (ROI-2) by setting a single detection threshold (gray dashed lines in the Ca^{2+} traces). Right column: zoom-in of the data in the gray boxes in the third column, showing detected Ca^{2+} sparks (*). (C) Left: input image; middle: 2-D heatmap of Ca^{2+} hotspots; right: 3-D representation of the heatmap emphasizing existence of hotspots of spark activity. Pseudocolors depict the number of frames in which $[Ca^{2+}]_i$ exceeded the detection threshold. Note that Ca^{2+} hotspots are predominantly found at the cell periphery. Dashes indicate cell outlines. Scale bar = 20 μm.

Please cite this article in press as: D. Visser, et al., TRPM7 triggers Ca^{2+} sparks and invadosome formation in neuroblastoma cells, Cell Calcium (2013), http://dx.doi.org/10.1016/j.ceca.2013.09.003

3.3. Automated background correction and Ca^{2+} spark detection

Initial results revealed that Ca^{2+} sparks were of low amplitude, whereas the background signal appeared non-uniform and showed slow fluctuations, due to variations in the TIRF illumination or focus (Video 1, Fig. 1A and B and Fig. S3A). This complicated detailed characterization and we therefore set out to optimize visualization and characterization by automating Ca^{2+} spark detection with ImageJ software.

First, we corrected the temporal background fluctuations by employing a running-background correction routine in which the background is updated dynamically in the time-series. A simple running-background correction in which frame $i-1$ serves as the background for frame i does not suffice because it would effectively truncate all Ca^{2+} sparks that last longer than one frame. We therefore designed a running background correction in which the background signal for frame i is calculated from the (pixelwise) minimal value of two frames before ($i-15$ and $i-5$) and two after ($i+5$ and $i+15$) that image. The range of ±5 and ±15 frames from image i was experimentally optimized to be close enough to accurately reflect any slow fluctuations in background and yet wide enough to minimize the chance that Ca^{2+} sparks would be present in all four background frames. Of several background correction algorithms tried, this one cleaned up the fluorescence signal most effectively and it emphasized only those intensity changes that corresponded to true Ca^{2+} sparks (Fig. 1A and B). In addition, we applied a 19×19 square kernel smoothing filter for visualization (but not for measurement) purposes. The line profiles and Ca^{2+} traces of selected Ca^{2+} sparks in Fig. 1A and B as well as the processed time-series in Video 2 and Fig. S3C illustrate the remarkable effectiveness of our running background-correction routine.

We next automated detection of Ca^{2+} sparks by applying a threshold that effectively segmented out Ca^{2+} sparks in the smoothed, background-corrected time series, yielding a binary mask (Video 3 and Fig. S3D and E). The spatial distribution and activity of Ca^{2+} sparks over time was finally captured in a single 'heatmap' by summing all thresholded mask images of the time-series. Thus, the heatmap reflects the number and localization of Ca^{2+} hotspots, with a single hotspot reporting the recurrence

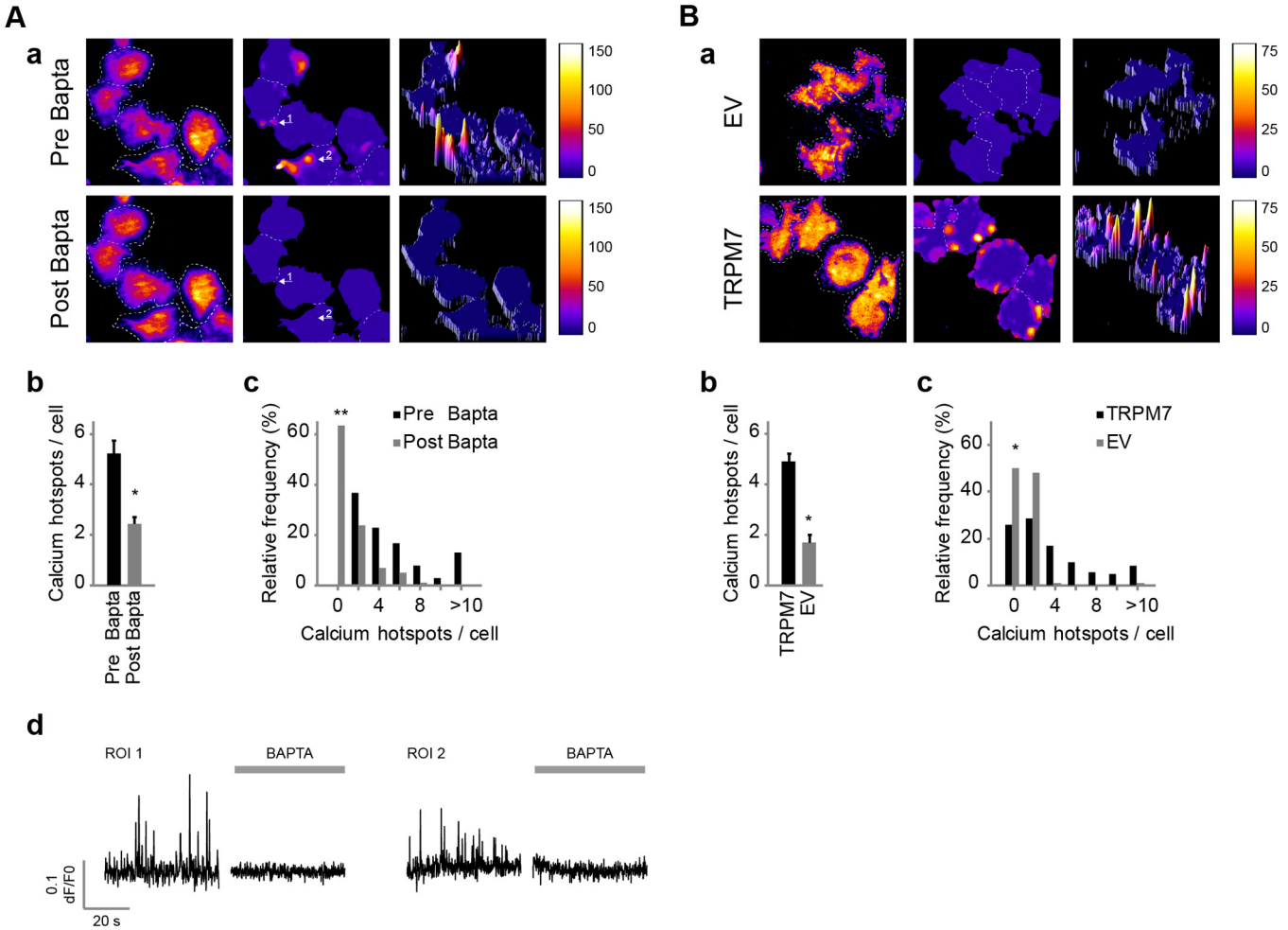

Fig. 2. Ca^{2+} sparking requires Ca^{2+} influx and correlates with TRPM7 expression levels. (A) N1E-115/TRPM7 cells loaded with Oregon Green 488 BAPTA-1-AM and EDTA-AM were imaged before and after the application of BAPTA. (a) Left: input image; middle and right, 2-D and 3-D heatmaps, respectively. Representative heatmaps of Ca^{2+} spark formation over time before (top) and after (bottom) application of BAPTA are depicted. For interpretation of heatmaps, see the legend of Fig. 1C and the text. (b) Average number of Ca^{2+} hotspots per cell before and after application of BAPTA ($n = 101$ [pre] and $n = 37$ [post], $p < 0.001$ versus pre; Mann–Whitney U-test, two-tailed). (c) Frequency histogram ($n = 101$, $p \ll 0.001$ versus pre, McNemar's test for paired proportions, two-tailed). (d) Ca^{2+} spark traces of representative Ca^{2+} hotspots (arrows in a) before (left) and after (right) BAPTA treatment. (B) N1E-115/TRPM7 cells were compared to their empty-vector controls with 3-fold lower TRPM7 expression. (a) Representative heatmaps of Ca^{2+} spark activity. (b) Mean number of Ca^{2+} hotspots per cell that showed Ca^{2+} sparking ($n = 58$ [N1E-115/EV] and $n = 202$ [N1E-115/TRPM7], $p < 0.001$; Mann–Whitney U-test, two-tailed). (c) Frequency distribution of sparking activity ($n = 116$ [N1E-115/EV], and $n = 272$ [N1E-115/TRPM7], $p < 0.001$; Fisher's exact test, two-tailed). Data in this figure represent mean ± SEM of at least 5 independent experiments. $^{*}p < 0.001$ and $^{**}p < 0.0001$.

Please cite this article in press as: D. Visser, et al., TRPM7 triggers Ca^{2+} sparks and invadosome formation in neuroblastoma cells, Cell Calcium (2013), http://dx.doi.org/10.1016/j.ceca.2013.09.003

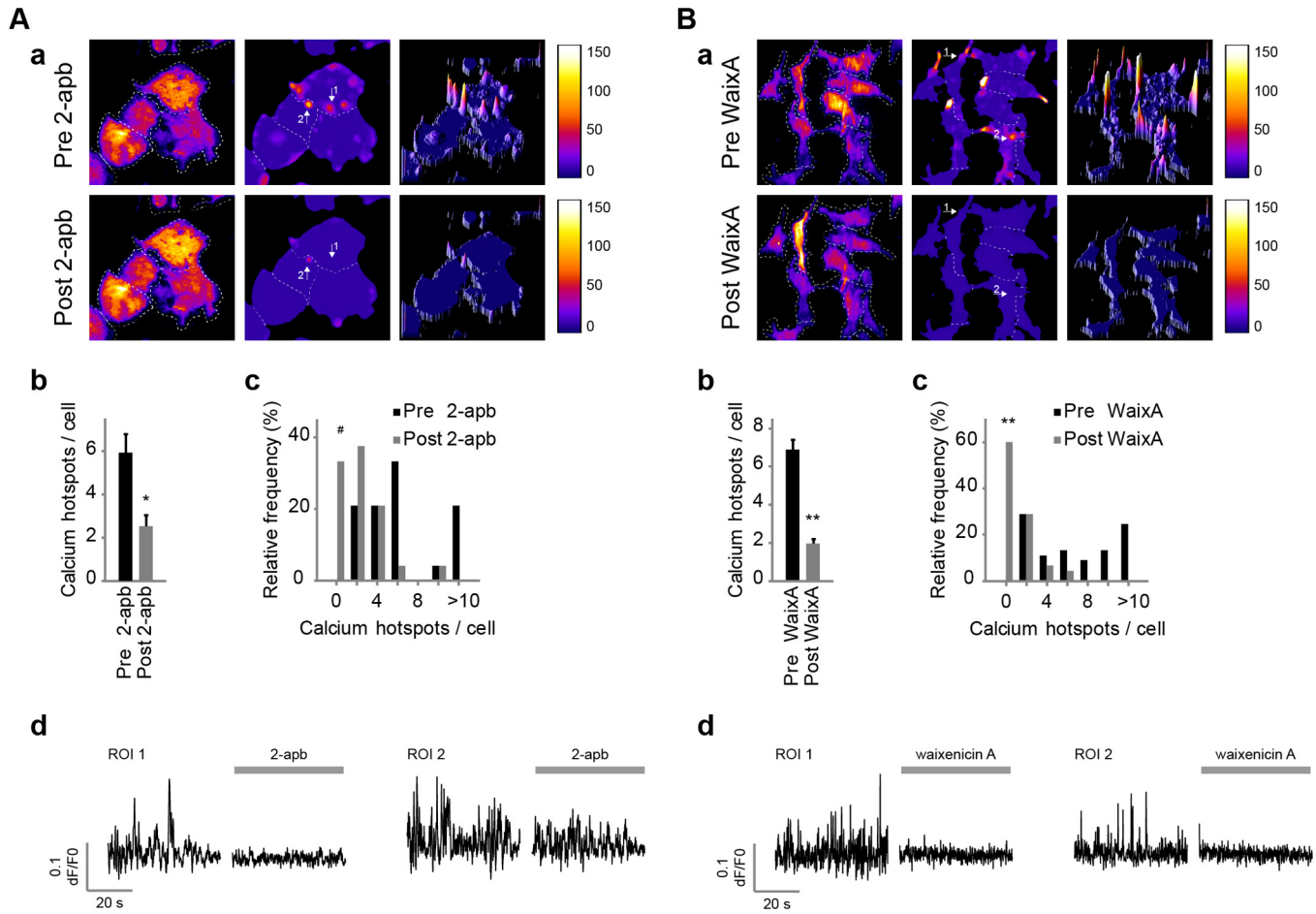

Fig. 3. Ca^{2+} sparks are mediated by TRPM7. Application of (A) 2-APB (100 μM) and (B) waixenicin-A (3–10 μM) inhibit TRPM7 and significantly reduce Ca^{2+} spark formation. (a) Heatmaps of Ca^{2+} sparking before (top) and after (bottom) application of inhibitors. (b) Number of Ca^{2+} hotspots per active cell (2-APB: $n = 24$ [pre] and $n = 17$ [post], $p < 0.001$; and waixenicin-A: $n = 45$ [pre] and $n = 20$ [post], $p \ll 0.001$; Mann–Whitney *U*-test, two-tailed). (c) Frequency distribution of number of hotspots per cell before and after application of inhibitors (2-APB: $n = 24$, $p < 0.01$; and waixenicin-A: $n = 45$, $p \ll 0.001$; McNemar's test for paired proportions, two-tailed). (d) Potent inhibition of Ca^{2+} spark activities at hotspots (indicated with arrows in a) following addition of 2-APB (see also Video 4) and waixenicin-A. Note that inhibition by waixenicin-A required preincubation for a few minutes. Data are mean ± SEM of at least 5 independent experiments. $^{\#}p < 0.01$, and $^{**}p < 0.0001$.

and duration of Ca^{2+} sparks (i.e. the number of frames a spark is detected in the series), but not their amplitude. Interestingly, this heatmap representation clearly highlighted subcellular locations with intense Ca^{2+} spark activity, that we will call 'Ca^{2+} hotspots' (Fig. 1C). Often, hotspots were most prominent at the cell periphery where most reorganization of the cytoskeleton occurs. Time courses of individual Ca^{2+} spark activity that were determined from regions of interest (ROI) in processed image stacks revealed that Ca^{2+} spark duration was generally highly variable, lasting between 0.1 s and ~5 s (median ~0.4 s), whereas spark amplitude ($\Delta F/F$) averaged 23% ± 12% ($N = 54$ ROIs and 146 sparks in 10 cells).

In conclusion, we worked out an image analysis routine to reliably and sensitively detect Ca^{2+} sparks. See Appendix A for a listing of the ImageJ macro, which will be available upon request.

3.4. Ca^{2+} sparks depend on Ca^{2+} influx and TRPM7 activity

Ca^{2+} signals may originate from either influx through ion channels in the plasma membrane or from internal stores. We first addressed whether Ca^{2+} sparks in N1E-115/TRPM7 cells require a plasma membrane component. Removal of extracellular free Ca^{2+} by chelation with BAPTA (4–8 mM) rapidly inhibited Ca^{2+} sparks (Fig. 2A), evidenced by the complete silencing of a significant proportion of active cells (63.4% decrease, $n = 101$, $p \ll 0.001$). The remaining cells showed a large decrease in number of Ca^{2+} hotspots per cell (53.6% ± 5.3% decrease, $n = 101$ cells [pre] and $n = 37$ cells [post], $p < 0.001$).

To determine whether TRPM7 is the membrane channel that mediated Ca^{2+} sparks we initially established that its expression levels correlate with Ca^{2+} spark activity (Fig. 2B). Since TRPM7 knockdown via RNA interference severely affects cell viability in this cell system (as well as many others [42,43]; and data not shown), we alternatively compared N1E-115/TRPM7 cells to the empty-vector control cells ('N1E-115/EV') that have 2–3 times lower expression of TRPM7 [20]. Indeed, N1E-115/EV cells appeared much less active, as both the percentage of cells that display Ca^{2+} sparks (N1E-115/TRPM7 = 74%, $n = 272$; N1E-115/EV = 50%, $n = 116$, $p < 0.001$) and the number of Ca^{2+} hotspots per active cell (1.69 ± 0.31 hotspots per control cell, $n = 58$, versus 4.9 ± 0.32 hotspots per TRPM7 overexpressing cell, $n = 202$, $p < 0.001$) were strongly decreased.

Furthermore, treatments known to affect TRPM7 permeation also affected Ca^{2+} sparking in N1E-115/TRPM7 cells. For example, application of 2-aminoethyl diphenylborinate (2-APB, 100 μM), which rapidly inhibits macroscopic TRPM7 Ca^{2+} signals ([36] and Fig. S4B), similarly abolished Ca^{2+} spark activity (Fig. 3 A and Video 4), decreasing Ca^{2+} hotspots by 57.2% ± 8.5% ($n = 24$ cells [pre] and $n = 17$ cells [post], $p < 0.001$) and completely preventing Ca^{2+} spark formation in 33.3% of previously active cells ($n = 24$, $p = 0.013$).

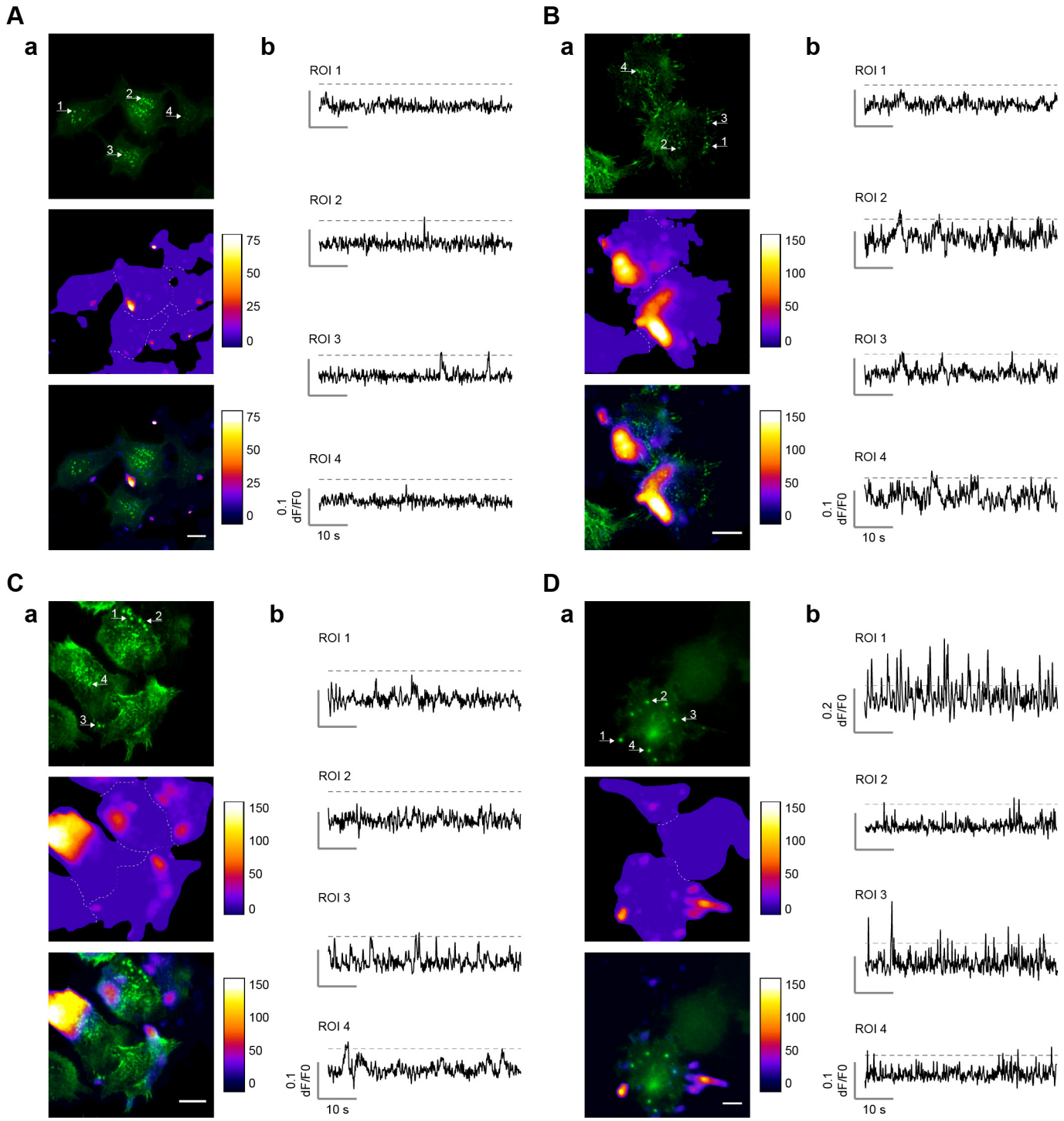

Fig. 4. Ca^{2+} hotspots do not localize specifically to invadosomes. (A)–(D) Four examples demonstrating the distribution of Ca^{2+} hotspots and invadosomes in N1E-115/TRPM7 cells. Invadosomes are visualized as bright actin dots, labeled with RFP-actin or Lifeact-dsRed (here in green). Shown in each panel is actin (top), Ca^{2+} hotspots (middle) and overlay (bottom). Please note that the minimum value of the LUT for the Ca^{2+} hotspot image in the overlay was adjusted to improve visualization of colocalization with invadosomes. Arrows indicate location of the Ca^{2+} traces in (b). In (A) Ca^{2+} hotspots are primarily located in the periphery, away from central invadosomes. In (B) Ca^{2+} hotspots appear along one side of the cell and are clearly excluded from invadosomes. In (C) several neighboring peripheral invadosomes (ROI 1 + 2) do not colocalize with Ca^{2+} hotspots. In (D) two peripheral invadosomes overlap with highly active Ca^{2+} hotspots (ROI 1 + 3), whereas others are mostly silent (ROI 2 + 4). As detailed in the text, statistical analysis reveals no significant colocalization of Ca^{2+} hotspots with invadosomes; thus, panels A–C are representative for the vast majority of observations whereas panel D presents a single outlier where some colocalization seems to occur. Scale bar = 20 μm.

In addition, increasing the extracellular concentration of Mg^{2+} to supraphysiological levels (10–20 mM) completely prevented Ca^{2+} spark formation in a significant proportion of previously active cells (37.2% decrease, $n = 86$, $p \ll 0.001$ versus pre-$MgCl_2$; McNemar's test for paired proportions, two-tailed) and diminished Ca^{2+} hotspots in the remainder of cells within several minutes post application ($n = 86$ [pre] and $n = 65$ [post], $p = 0.123$; Mann–Whitney *U*-test, two-tailed). Hence, our data indicate that Ca^{2+} influx through the TRPM7 pore underlies Ca^{2+} spark activity in N1E-115/TRPM7 cells.

Please cite this article in press as: D. Visser, et al., TRPM7 triggers Ca^{2+} sparks and invadosome formation in neuroblastoma cells, Cell Calcium (2013), http://dx.doi.org/10.1016/j.ceca.2013.09.003

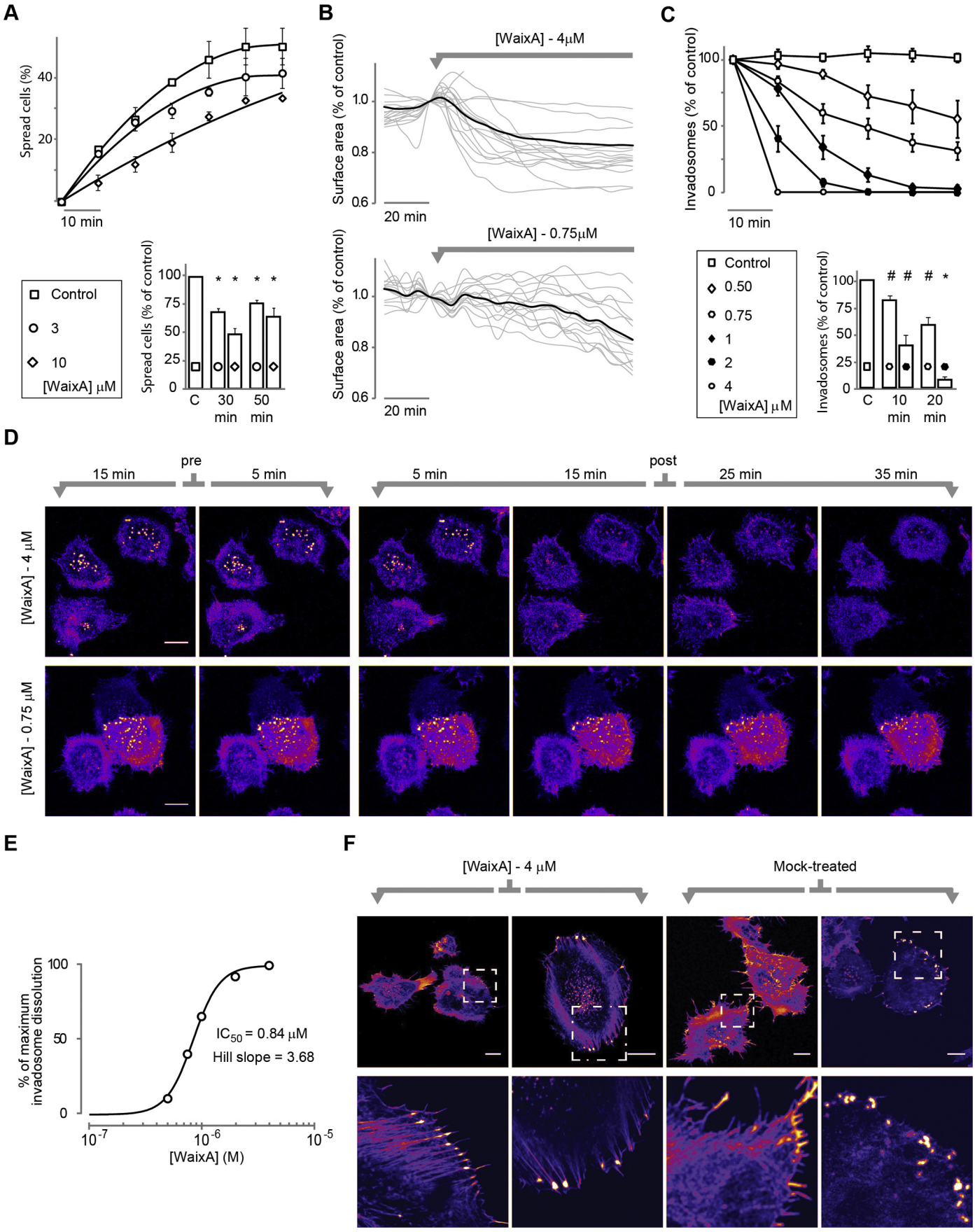
A
Spread cells (%)
10 min
Control
3
10
[WaixA] μM
Spread cells (% of control)
C
30 min
50 min
B
[WaixA] - 4μM
Surface area (% of control)
20 min
[WaixA] - 0.75μM
C
Invadosomes (% of control)
10 min
Control
0.50
0.75
1
2
4
[WaixA] μM
C
10 min
20 min
D
15 min
pre
5 min
5 min
15 min
post
25 min
35 min
[WaixA] - 4 μM
[WaixA] - 0.75 μM
E
% of maximum invadosome dissolution
IC50 = 0.84 μM
Hill slope = 3.68
[WaixA] (M)
F
[WaixA] - 4 μM
Mock-treated

3.5. Waixenicin-A blockage of Ca^{2+} spark activity

While 2-APB rapidly blocks Ca^{2+} influx through TRPM7, it also is known to affect other Ca^{2+} channels including I_{CRAC} and IP_3 receptors. We therefore turned our attention to waixenicin-A, a metabolite isolated from extracts of the soft coral *S. edmondsoni*, which potently and specifically inhibits TRPM7 channels [44,45]. Although it is currently not clear whether this is due to pore blockage or perhaps through other mechanism(s) that involve binding of the compound to TRPM7, waixenicin-A is, to date, considered the most specific inhibitor of this channel. In line with these reports, pre-incubation with waixenicin-A completely prevented the characteristic TRPM7-dependent sustained Ca^{2+}-influx phase upon BK-stimulation, as illustrated by Ca^{2+} fluorometry experiments (Fig. S4C). Waixenicin-A treatment also strongly suppressed Ca^{2+} sparking (Fig. 3B), apparent from both a large drop in the fraction of cells that exhibit Ca^{2+} sparks (60% decrease, $n = 45$, $p \ll 0.001$) and from the strongly decreased number of Ca^{2+} hotspots in the remaining active cells (71.7% ± 5.5% decrease, $n = 45$ cells, $p \ll 0.001$). Taken together, these data clearly establish TRPM7 as the carrier of Ca^{2+}-influx in our cells.

3.6. Ca^{2+} sparks do not localize to invadosomes

To address the potential contribution of TRPM7-mediated Ca^{2+} sparks to invadosome dynamics, we set out to track Ca^{2+} spark activity and invadosomes simultaneously. Invadosomes are conveniently visualized by monitoring their actin-dense core with actin markers such as mRFP-actin or Lifeact-dsRed. The very intense staining of both these markers in invadosome cores overlaps well with known invadosome markers like vinculin, Tks4 and cortactin [46,47] (Fig. S1A and data not shown). We confirmed that both markers did not affect Ca^{2+} spark formation (4.3 ± 0.6 and 4.6 ± 0.7 Ca^{2+} hotspots per cell, untransfected-control, $n = 54$, versus RFP-actin-transfected, $n = 31$, respectively, $p = 0.73$, Mann–Whitney parameter free test, 2-tailed; results obtained with Lifeact-dsRed were similar but not quantified in detail). We also checked that invadosome formation, numbers, architecture and dynamics were unaffected by the conditions used to visualize Ca^{2+} sparks, i.e. by preincubation with EDTA-AM (Fig. S5).

As mentioned before, in those experiments Ca^{2+} sparks appeared mostly absent from the cell center and were found almost exclusively at the periphery where dynamic actin remodeling takes place (see Figs. 1C, 2 and 3). TRPM7-mediated Ca^{2+} sparks are, therefore, unlikely to contribute considerably to formation and turnover of central invadosomes (see Fig. S1A), and indeed no evidence for significant colocalization of Ca^{2+} sparks with central invadosomes was found (Fig. 4A and B).

Since immuno-localization showed that TRPM7 was more apparent in peripheral invadosomes (see Fig. S1C) we expected that Ca^{2+} sparking would be more pronounced at those sites, but detailed analysis showed that this was not the case. In the vast majority of experiments we found no evidence for colocalization of Ca^{2+} hotspots with peripheral invadosomes at all (Fig. 4B–D). Occasionally we observed some overlap of Ca^{2+} sparks with peripheral invadosomes (Fig. 4D), but these events represented a minor proportion of the studied peripheral invadosomes. Statistical analyses revealed that ~92% of detected Ca^{2+} hotspots ($n = 107$) were outside invadosomes whereas conversely, only ~11% of studied invadosomes showed Ca^{2+} spark activity ($n = 79$). Since we calculated that the footprint of Ca^{2+} hotspots in a cell on average covers ~17% of the total cell surface (mean ± SEM; cell size = 1309 ± 61.3 μm^2, $n = 96$; Ca^{2+} hotspot size = 43.6 ± 6.4 μm^2, $n = 178$; Ca^{2+} hotspots per cell = 4.9 ± 0.32, $n = 202$), the probability of randomly observing at least 11% of invadosomes with Ca^{2+} spark activity ($n = 79$) is very high ($P_{0.17}(x \geq 11\%) = 0.93$). Moreover, we did not observe any invadosomes that formed or disappeared at Ca^{2+} hotspots during, prior to or following Ca^{2+} spark ignition.

In summary, despite the extensive numbers of cells and invadosomes that we studied, we found no evidence in support of our hypothesis that TRPM7 serves to set up a local microenvironment of increased Ca^{2+} levels in invadosomes. We therefore have to reject the hypothesis that TRPM7 controls invadosome dynamics via localized Ca^{2+} signals.

3.7. Cytosolic Ca^{2+} levels and invadosomes

Apart from mediating Ca^{2+} sparks, TRPM7 expression has also been shown to affect basal Ca^{2+} levels in N1E-115 cells [20,36]. Buffering of extracellular Ca^{2+} by BAPTA (2–8 mM) to nanomolar levels not only inhibited Ca^{2+} sparking (Fig. 2A) but also reverted the increase of basal Ca^{2+} levels that is apparent in N1E-115/TRPM7 cells ([36] and Fig. S4A). Could such Ca^{2+} changes at a more global (cell-wide) scale, rather than in the invadosome microenvironment, somehow affect invadosome dynamics? We assayed invadosome dynamics by recording confocal time-lapse movies of cells expressing GFP-actin or Lifeact-GFP over prolonged times. Strikingly, addition of BAPTA (2–8 mM) failed to noticeably affect invadosome formation or turnover ($n = 36$ time-lapse recordings in 6 separate experiments) (Video 5). Similar results were obtained with the Ca^{2+} chelator EGTA, or when the imaging buffer was replaced by nominally Ca^{2+}-free solution (data not shown). This demonstrates that like the TRPM7-mediated Ca^{2+} sparks, also the effects of TRPM7 expression on basal Ca^{2+} levels are not involved in regulating invadosome dynamics. As expected from the essential role of extracellular Ca^{2+} in cell adhesion [48,49], cells eventually detached when exposed to nominally free Ca^{2+} buffer for prolonged periods of time, i.e. 8 h. However, most of those cells that were still adherent after such treatment did contain invadosomes ($n = 60$ fields of cells in 6 separate experiments) (Fig. S6). This is notable because the examination time point, 8 h post BAPTA-treatment, well exceeds the average lifetime of invadosomes (up to a few hours) in these cells. The presence of invadosomes at this time point, therefore, indicates that neither local Ca^{2+} sparking, nor basal Ca^{2+} levels are dominant in the regulation of invadosomes in these cells.

Fig. 5. Waixenicin-A treatment reverts TRPM7-mediated cell spreading and actomyosin-relaxation. (A) Top: effect of waixenicin-A treatment on cell spreading upon seeding. Bottom: quantification (mean ± SEM) of initial spreading at 30 and 50 min ($p < 0.001$ versus control, one-sample *t*-test. Experiments were repeated 5 times independently, each for at least 10 fields of view per condition). (B) Waixenicin-A causes cell contraction. Cell surface area was tracked over time by image analysis before and after application of waixenicin-A (0.75 μM and 4 μM). Traces (black, average response; gray, individual responses) were normalized to the cell surface area at the frame before application. (C) Top: effect of waixenicin-A treatment (added at $t = 0$) on invadosome numbers. Bottom: quantification (mean ± SEM) of invadosome dissolution at 10 and 20 min after application (2 μM, $n = 5$ fields of view; 0.75 μM, $n = 15$, counting hundreds of invadosomes per data point, $p < 0.005$ versus control, one-sample *t*-test). (D) Typical examples of confocal time-series experiments that show concentration-dependent invadosome dissolution upon waixenicin-A treatment (0.75 μM and 4 μM) in N1E-115/TRPM7 cells that stably express GFP-actin (see also Video 6). (E) Dose–response curve derived from the data in (C) at 20 min after application. (F) Examples of adherent N1E-115/TRPM7 cells treated with waixenicin-A (4 μM) or vehicle for 24 h. F-actin stained with Phalloidin-Alexa568. Note the induction of focal adhesions and stress fibers upon exposure to waixenicin-A (see zoom-in). Scalebar = 20 μm. $^{*}p < 0.001$ and $^{\#}p < 0.005$.

Please cite this article in press as: D. Visser, et al., TRPM7 triggers Ca^{2+} sparks and invadosome formation in neuroblastoma cells, Cell Calcium (2013), http://dx.doi.org/10.1016/j.ceca.2013.09.003

3.8. Effect of waixenicin-A on cellular contractility and adhesion

The role of TRPM7 channels in controlling cell adhesion and migration has been well established in a range of different cell types [7,20,31,32,34,50,51]. In N1E-115 cells, the most prominent effects of TRPM7 upregulation are an increase in basal Ca^{2+} levels and relaxation of the cytoskeleton, which leads to a spread phenotype and the formation of invadosomes [20]. However, although TRPM7 localizes to invadosomes ([20] and Fig. S1C), our experiments show that Ca^{2+} levels play no dominant role in determining invadosome dynamics in these cells (Fig. 4 and Fig. S6). Experiments we carried out with waixenicin-A may shed some light on this apparent contradiction. When testing the effects of waixenicin-A on cytoskeletal organization of N1E-115/TRPM7 cells, we noted that initial spreading after seeding of cells was impaired in the presence of waixenicin-A (25–50% decrease compared to control, $p < 0.001$; $n = 5$ experiments; Fig. 5A). Conversely, N1E-115/TRPM7 cells that were allowed to adhere and spread to coverslips in serum-containing DMEM showed a mild contraction response within minutes after addition of waixenicin-A, indicative of increased cellular tension (Fig. 5B). This response was concentration dependent and typically proceeded slowly at lower concentrations (10% loss of surface area for 4 μM and 0.75 μM was 25 and 70 min, respectively; Fig. 5B). Even more striking was the effect of waixenicin-A on invadosomes. Addition of high doses (≥2 μM) of waixenicin-A caused a very marked, rapid and complete dissolution of invadosomes (Fig. 5C and D) which typically was complete within 10 min, as assayed by live-cell imaging. At lower doses changes progressed more gradually with clear effects still present at doses as low as 0.5 μM (Fig. 5C and D and Video 6). The dose–response curve (taken at 20 min post addition of waixenicin-A; Fig. 5E) reveals an IC_{50} of 0.84 μM and appears quite steep. We therefore analyzed for cooperativity by Hill slope analysis, which revealed a Hill coefficient of 3.68, i.e. close to 4. It is therefore tempting to speculate that the steep dose–response curve reflects binding of one molecule of waixenicin-A to each of the four subunits of the TRPM7 channel, although direct evidence for this notion is lacking. In any case, the rapid disappearance of invadosomes following TRPM7 inhibition is in agreement with the notion that TRPM7-mediated loss of actomyosin contractility regulates invadosome formation and turnover [12,13]. To further test this, we assayed cells at 24–48 h post waixenicin-A treatment. Indeed, the majority of cells showed extensive formation of focal adhesions and stress fibers at these late time points (Fig. 5F), indicating increased cellular tension [52]. Hence, waixenicin-A appears to revert the morphological phenotype of TRPM7 overexpression in N1E-115. We also conclude that waixenicin-A is a promising and powerful pharmacological tool to study the effects of TRPM7 on adhesion and migration.

In summary, these data support the view that TRPM7 activity affects the tension-relaxation balance of the actomyosin cytoskeleton, which in turn modulates the formation of various adhesion structures. Strikingly, however, the effect of waixenicin-A appears independent of Ca^{2+} influx through the TRPM7 channel.

4. Discussion

There is ample evidence that ion channels can set up intracellular Ca^{2+} microdomains to locally regulate effector proteins. Synaptic transmission in neurons provides a clear example of such a model [53]. N- and P/Q-type voltage-operated Ca^{2+} channels in synaptic terminals generate brief and localized Ca^{2+} transients that activate the SNARE-complex to initiate neurotransmitter release [54–56]. In the present study we focused on the role of such Ca^{2+} sparks in the control of cell adhesion dynamics, in particular of invadosomes in neuroblastoma cells. Expression levels of the Ca^{2+}-permeable divalent cation channel TRPM7 are known to affect adhesion and migration [20,31–34,50,51,57], and we have shown that the channel localizes to a ring around invadosomes ([20] and Fig. S1C and D). Such a constellation theoretically constitutes the ideal architecture to generate local Ca^{2+} signals, and indeed a variety of Ca^{2+} sensitive regulatory proteins have been identified in invadosomes [9,19–21,58]. We addressed the hypothesis that TRPM7 exerts its effect on adhesion dynamics by mediating local Ca^{2+} signals so as to modulate Ca^{2+}-sensitive cytoskeletal effector proteins. TRPM7 itself may be one of the effectors because Ca^{2+} influx through the channel appears to be required for the association of its kinase domain with the myosin II heavy chain [20,30].

To address our hypothesis we developed a sensitive assay that greatly improves the visualization of local Ca^{2+} signals and reliably detects them at a high spatiotemporal resolution. Our data indicate that TRPM7 indeed plays an essential role in mediating localized Ca^{2+} sparks at the basal membrane of neuroblastoma cells. Ca^{2+} hotspots are prevalent at the periphery of the cells. However, despite the sensitivity of our analysis we only sporadically detected such Ca^{2+} sparks at invadosomes, and overall the spatial distribution of Ca^{2+} hotspots showed no enrichment in invadosomes. Thus, our study dissociates TRPM7-mediated Ca^{2+} sparking from invadosome dynamics and actomyosin contractility.

Remarkably, inhibition of TRPM7 with waixenicin-A (but not interfering with Ca^{2+} influx by chelation of extracellular Ca^{2+}) caused rapid and complete dissolution of invadosomes and, on a longer timescale, induced a more contractile phenotype in neuroblastoma cells, as evidenced from the development of numerous FAs and stress fibers. How waixenicin-A causes this effect, in a manner unrelated to Ca^{2+} influx, remains to be investigated. We previously reported that phosphotransferase-activity of TRPM7's kinase domain was not required for the induction of cell spreading, as evident by using a kinase-dead mutant (D1775A), and suggested that this instead may be caused by altered signaling through elevated basal $[Ca^{2+}]_i$ [20], but our current data show that this latter viewpoint requires revision. Yet another model was put forward by Su and colleagues, who proposed that TRPM7 modulates the actomyosin cytoskeleton and its contractility by regulating $[Mg^{2+}]_i$ [32]. Indeed, TRPM7 channels readily carry Mg^{2+} ions too, but at least in our cells, waixenicin-A induced alterations in Mg^{2+} influx cannot be held responsible for the observed cytoskeletal effects because its chelation with 10 mM EDTA was without effect (data not shown). Alternatively, we should consider the possibility that waixenicin-A may alter interactions of TRPM7 with other proteins or may even induce endocytosis of TRPM7, thereby affecting its proposed scaffolding function. Lastly, we cannot fully exclude the possibility that waixenicin-A may have off-target effects, although a previous study reported that waixenicin-A did not affect other ion channels (including TRP members and CRAC) at concentrations well-above those employed in the current study [44]. In any case, the responses observed upon application of waixenicin-A resemble that of TRPM7 knockdown in MDA-MB-231 breast cancer cells [34] and generally are in line with the notion that TRPM7 expression levels affect cytoskeletal organization and cellular tension [20,32,34]. Cellular tension is an important determinant of tumor cell transformation and malignancy (e.g. [59,60]) and indeed, TRPM7 has recently been implicated in breast cancer metastasis [34] and high expression is associated with adverse pathological parameters [57,61].

Several recent studies have addressed the possible role of localized Ca^{2+} signals in the turnover of adhesion sites. Our identification of a key role for TRPM7 in the ignition of Ca^{2+} sparks is in line with the results of Wei and colleagues, who showed by knockdown and inhibitor studies that TRPM7-mediated Ca^{2+} 'flickering' is involved in guiding of fibroblast lamellipodia during directional migration experiments. They presented a model in which TRPM7,

together with type 2 IP_3 receptors, evokes Ca^{2+} sparks at the leading edge of migrating fibroblasts and argue that those events are involved in the regulation of traction forces that are associated with migration [7]. Whether or not the Ca^{2+} sparks in their study modify the dynamics of FAs, and which effector proteins are affected remains to be determined. In another recent study, TRPV2 channels were demonstrated to localize to invadosomes in macrophages [19]. This study showed that fMLP-induced Ca^{2+} influx through TRPV2 triggered dissolution of invadosomes through activation of the Ca^{2+}-sensitive protein tyrosine kinase Pyk2 [19] but it did not focus on resolving local Ca^{2+} microdomains.

Whereas thus the existence and exact role of localized Ca^{2+} signals in adhesive structures in various cell types may be debated, it has become clear that invadosomes contain a number of Ca^{2+}-sensitive protein constituents, including myosins, gelsolin, tropomyosins, calponin and vinculin. In microglial invadosomes the Ca^{2+} release activated channel (CRAC) Orai1 was identified [21] and inhibitor studies suggested a function in formation of these structures. Notably, this study found no evidence for a role of TRPM7 (or other TRP channels tested) in invadosome formation. In addition, the authors identified calmodulin as a prominent constituent in invadosomes. This small Ca^{2+} binding protein conveys Ca^{2+} sensitivity to its (many) protein interactors, among which are several TRP channels [62] and cytoskeletal regulators, and thus is a critical determinant of Ca^{2+} signaling [63,64].

In summary, functional studies providing evidence for the invadosome as a hub for localized Ca^{2+} signaling have been very limited, and indeed consensus on the importance of Ca^{2+} in general (be it localized Ca^{2+} influx, cytosolic Ca^{2+} levels or extracellular Ca^{2+}) for invadosome dynamics has not been reached. For example, Ca^{2+} influx may trigger invadosome dissolution in some studies [19,65] and it was required for invadosome formation in others [21], whereas we here describe that switching to nominal $[Ca^{2+}]_e$ does not noticeably affect de novo formation or dynamic behavior of invadosomes. In addition to the different experimental strategies employed in these studies, it may be anticipated that cell-type specific differences govern the variation in these results. As to how TRPM7 controls the actomyosin cytoskeleton and cell adhesion dynamics, either the activity of its kinase-domain [20,66] as well as Ca^{2+}-influx [7,20,31,33] and Mg^{2+}-influx [32,50] through its pore have been proposed. Based on the results of the present study we conclude that TRPM7 regulates invadosome dynamics by affecting actomyosin-based tension conditions in adherent cells independent of (localized) Ca^{2+} influx. Just how interfering with TRPM7 functioning exerts these effects remains a challenge for future research.

Conflict of interest

The authors declare that they have no conflict of interest.

Ethical standards

The authors declare that all experiments comply with Dutch and American laws.

Acknowledgements

We thank Dr. W. Moolenaar and J. Middelbeek for critical reading of the manuscript and members of our department for discussion. Dr. L. Oomen and L. Brocks are acknowledged for help with TIRF microscopy, and Mr. D. Cagle is thanked for assistance in isolating waixeincin-A. This work was supported by Koningin Wilhelmina Fonds grants KUN2007-3733 and NKI 2010-4626 (to FNvL and KJ), by a Nederlandse Organisatie voor Wetenschappelijk Onderzoek investment grant (to KJ), and by National Institutes of Health grants P20 GM-103466-11 (to FDH) and P01 GM078195 (to AF).

Appendix A. Supplementary data

Supplementary data associated with this article can be found, in the online version, at http://dx.doi.org/10.1016/j.ceca.2013.09.003.

References

[1] I. Kaverina, O. Krylyshkina, J.V. Small, Regulation of substrate adhesion dynamics during cell motility, Int. J. Biochem. Cell Biol. 34 (2002) 746–761.
[2] K. Rottner, T.E. Stradal, Actin dynamics and turnover in cell motility, Curr. Opin. Cell Biol. 23 (2011) 569–578.
[3] A.J. Ridley, M.A. Schwartz, K. Burridge, R.A. Firtel, M.H. Ginsberg, G. Borisy, J.T. Parsons, A.R. Horwitz, Cell migration: integrating signals from front to back, Science 302 (2003) 1704–1709.
[4] G. Burgstaller, M. Gimona, Actin cytoskeleton remodelling via local inhibition of contractility at discrete microdomains, J. Cell Sci. 117 (2004) 223–231.
[5] Y. Fukata, M. Amano, K. Kaibuchi, Rho-Rho-kinase pathway in smooth muscle contraction and cytoskeletal reorganization of non-muscle cells, Trends Pharmacol. Sci. 22 (2001) 32–39.
[6] K. Burridge, K. Wennerberg, Rho and Rac take center stage, Cell 116 (2004) 167–179.
[7] C. Wei, X. Wang, M. Chen, K. Ouyang, L.S. Song, H. Cheng, Calcium flickers steer cell migration, Nature 457 (2009) 901–905.
[8] F.C. Tsai, T. Meyer, Ca(2+) pulses control local cycles of lamellipodia retraction and adhesion along the front of migrating cells, Curr. Biol. 22 (2012) 837–842.
[9] S. Linder, C. Wiesner, M. Himmel, Degrading devices: invadosomes in proteolytic cell invasion, Annu. Rev. Cell Dev. Biol. 27 (2011) 185–211.
[10] O. Collin, S. Na, F. Chowdhury, M. Hong, M.E. Shin, F. Wang, N. Wang, Self-organized podosomes are dynamic mechanosensors, Curr. Biol. 18 (2008) 1288–1294.
[11] D.A. Murphy, S.A. Courtneidge, The 'ins' and 'outs' of podosomes and invadopodia: characteristics, formation and function, Nat. Rev. Mol. Cell Biol. 12 (2011) 413–426.
[12] S.F. van Helden, M.M. Oud, B. Joosten, N. Peterse, C.G. Figdor, F.N. van Leeuwen, PGE2-mediated podosome loss in dendritic cells is dependent on actomyosin contraction downstream of the RhoA-Rho-kinase axis, J. Cell Sci. 121 (2008) 1096–1106.
[13] T. Lener, G. Burgstaller, L. Crimaldi, S. Lach, M. Gimona, Matrix-degrading podosomes in smooth muscle cells, Eur. J. Cell Biol. 85 (2006) 183–189.
[14] K. van den Dries, S.F. van Helden, J.T. Riet, R. Diez-Ahedo, C. Manzo, M.M. Oud, F.N. van Leeuwen, R. Brock, M.F. Garcia-Parajo, A. Cambi, et al., Geometry sensing by dendritic cells dictates spatial organization and PGE(2)-induced dissolution of podosomes, Cell Mol. Life Sci. 69 (2012) 1889–1901.
[15] D. Geblinger, C. Zink, N.D. Spencer, L. Addadi, B. Geiger, Effects of surface microtopography on the assembly of the osteoclast resorption apparatus, J. R. Soc. Interface 9 (2012) 1599–1608.
[16] K. Harper, D. Arsenault, S. Boulay-Jean, A. Lauzier, F. Lucien, C.M. Dubois, Autotaxin promotes cancer invasion via the lysophosphatidic acid receptor 4: participation of the cyclic AMP/EPAC/Rac1 signaling pathway in invadopodia formation, Cancer Res. 70 (2010) 4634–4643.
[17] P. Rottiers, F. Saltel, T. Daubon, B. Chaigne-Delalande, V. Tridon, C. Billottet, E. Reuzeau, E. Genot, TGFbeta-induced endothelial podosomes mediate basement membrane collagen degradation in arterial vessels, J. Cell Sci. 122 (2009) 4311–4318.
[18] V. Desmarais, H. Yamaguchi, M. Oser, L. Soon, G. Mouneimne, C. Sarmiento, R. Eddy, J. Condeelis, N-WASP and cortactin are involved in invadopodium-dependent chemotaxis to EGF in breast tumor cells, Cell Motil. Cytoskeleton 66 (2009) 303–316.
[19] M. Nagasawa, I. Kojima, Translocation of calcium-permeable TRPV2 channel to the podosome: its role in the regulation of podosome assembly, Cell Calcium 51 (2012) 186–193.
[20] K. Clark, M. Langeslag, B. van Leeuwen, L. Ran, A.G. Ryazanov, C.G. Figdor, W.H. Moolenaar, K. Jalink, F.N. van Leeuwen, TRPM7, a novel regulator of actomyosin contractility and cell adhesion, EMBO J. 25 (2006) 290–301.
[21] T.A. Siddiqui, S. Lively, C. Vincent, L.C. Schlichter, Regulation of podosome formation, microglial migration and invasion by Ca^{2+}-signaling molecules expressed in podosomes, J. Neuroinflammation 9 (2012) 250.
[22] N. Damann, T. Voets, B. Nilius, TRPs in our senses, Curr. Biol. 18 (2008) R880–R889.
[23] A.P. Christensen, D.P. Corey, TRP channels in mechanosensation: direct or indirect activation? Nat. Rev. Neurosci. 8 (2007) 510–521.
[24] T. Numata, T. Shimizu, Y. Okada, TRPM7 is a stretch- and swelling-activated cation channel involved in volume regulation in human epithelial cells, Am. J. Physiol. Cell Physiol. 292 (2007) C460–C467.
[25] E. Oancea, J.T. Wolfe, D.E. Clapham, Functional TRPM7 channels accumulate at the plasma membrane in response to fluid flow, Circ. Res. 98 (2006) 245–253.
[26] L.W. Runnels, L. Yue, D.E. Clapham, TRP-PLIK, a bifunctional protein with kinase and ion channel activities, Science 291 (2001) 1043–1047.

[27] M.J. Nadler, M.C. Hermosura, K. Inabe, A.L. Perraud, Q. Zhu, A.J. Stokes, T. Kurosaki, J.P. Kinet, R. Penner, A.M. Scharenberg, et al., LTRPC7 is a Mg.ATP-regulated divalent cation channel required for cell viability, Nature 411 (2001) 590–595.
[28] L.V. Ryazanova, K.S. Pavur, A.N. Petrov, M.V. Dorovkov, A.G. Ryazanov, Novel type of signaling molecules: protein kinases covalently linked with ion channels, Mol. Biol. 35 (2001) 271–283.
[29] M.V. Dorovkov, A.G. Ryazanov, Phosphorylation of annexin I by TRPM7 channel-kinase, J. Biol. Chem. 279 (2004) 50643–50646.
[30] K. Clark, J. Middelbeek, M.V. Dorovkov, C.G. Figdor, A.G. Ryazanov, E. Lasonder, F.N. van Leeuwen, The alpha-kinases TRPM6 and TRPM7, but not eEF-2 kinase, phosphorylate the assembly domain of myosin IIA, IIB and IIC, FEBS Lett. 582 (2008) 2993–2997.
[31] L.T. Su, M.A. Agapito, M. Li, W.T. Simonson, A. Huttenlocher, R. Habas, L. Yue, L.W. Runnels, TRPM7 regulates cell adhesion by controlling the calcium-dependent protease calpain, J. Biol. Chem. 281 (2006) 11260–11270.
[32] L.T. Su, W. Liu, H.C. Chen, O. Gonzalez-Pagan, R. Habas, L.W. Runnels, TRPM7 regulates polarized cell movements, Biochem. J. 434 (2011) 513–521.
[33] J.P. Chen, Y. Luan, C.X. You, X.H. Chen, R.C. Luo, R. Li, TRPM7 regulates the migration of human nasopharyngeal carcinoma cell by mediating Ca(2+) influx, Cell Calcium 47 (2010) 425–432.
[34] J. Middelbeek, A.J. Kuipers, L. Henneman, D. Visser, I. Eidhof, R. van Horssen, B. Wieringa, S.V. Canisius, W. Zwart, L.F. Wessels, et al., TRPM7 is required for breast tumor cell metastasis, Cancer Res. 72 (2012) 4250–4261.
[35] E. Fonfria, P.R. Murdock, F.S. Cusdin, C.D. Benham, R.E. Kelsell, S. McNulty, Tissue distribution profiles of the human TRPM cation channel family, J. Recept. Signal Transduct. Res. 26 (2006) 159–178.
[36] M. Langeslag, K. Clark, W.H. Moolenaar, F.N. van Leeuwen, K. Jalink, Activation of TRPM7 channels by phospholipase C-coupled receptor agonists, J. Biol. Chem. 282 (2007) 232–239.
[37] H. Cheng, W.J. Lederer, Calcium sparks, Physiol. Rev. 88 (2008) 1491–1545.
[38] R.Y. Tsien, New calcium indicators and buffers with high selectivity against magnesium and protons: design, synthesis, and properties of prototype structures, Biochemistry 19 (1980) 2396–2404.
[39] R.M. Luik, M.M. Wu, J. Buchanan, R.S. Lewis, The elementary unit of store-operated Ca^{2+} entry: local activation of CRAC channels by STIM1 at ER-plasma membrane junctions, J. Cell Biol. 174 (2006) 815–825.
[40] D. Zenisek, V. Davila, L. Wan, W. Almers, Imaging calcium entry sites and ribbon structures in two presynaptic cells, J. Neurosci. 23 (2003) 2538–2548.
[41] L.S. Song, J.S. Sham, M.D. Stern, E.G. Lakatta, H. Cheng, Direct measurement of SR release flux by tracking 'Ca^{2+} spikes' in rat cardiac myocytes, J. Physiol. 512 (Pt 3) (1998) 677–691.
[42] R.C. Wykes, M. Lee, S.M. Duffy, W. Yang, E.P. Seward, P. Bradding, Functional transient receptor potential melastatin 7 channels are critical for human mast cell survival, J. Immunol. 179 (2007) 4045–4052.
[43] T. Hanano, Y. Hara, J. Shi, H. Morita, C. Umebayashi, E. Mori, H. Sumimoto, Y. Ito, Y. Mori, R. Inoue, Involvement of TRPM7 in cell growth as a spontaneously activated Ca^{2+} entry pathway in human retinoblastoma cells, J. Pharmacol. Sci. 95 (2004) 403–419.
[44] S. Zierler, G. Yao, Z. Zhang, W.C. Kuo, P. Porzgen, R. Penner, F.D. Horgen, A. Fleig, Waixenicin A inhibits cell proliferation through magnesium-dependent block of transient receptor potential melastatin 7 (TRPM7) channels, J. Biol. Chem. 286 (2011) 39328–39335.
[45] B.J. Kim, J.H. Nam, Y.K. Kwon, I. So, S.J. Kim, The role of waixenicin a as transient receptor potential melastatin 7 blocker, Basic Clin. Pharmacol. Toxicol. 112 (2013) 83–89.
[46] M.D. Buschman, P.A. Bromann, P. Cejudo-Martin, F. Wen, I. Pass, S.A. Courtneidge, The novel adaptor protein Tks4 (SH3PXD2B) is required for functional podosome formation, Mol. Biol. Cell 20 (2009) 1302–1311.
[47] M. Oser, H. Yamaguchi, C.C. Mader, J.J. Bravo-Cordero, M. Arias, X. Chen, V. Desmarais, J. van Rheenen, A.J. Koleske, J. Condeelis, Cortactin regulates cofilin and N-WASp activities to control the stages of invadopodium assembly and maturation, J. Cell Biol. 186 (2009) 571–587.
[48] M.D. Sjaastad, W.J. Nelson, Integrin-mediated calcium signaling and regulation of cell adhesion by intracellular calcium, Bioessays 19 (1997) 47–55.
[49] E.A. Cox, A. Huttenlocher, Regulation of integrin-mediated adhesion during cell migration, Microsc. Res. Tech. 43 (1998) 412–419.
[50] E. Abed, R. Moreau, Importance of melastatin-like transient receptor potential 7 and magnesium in the stimulation of osteoblast proliferation and migration by platelet-derived growth factor, Am. J. Physiol. Cell Physiol. 297 (2009) C360–C368.
[51] H. Gao, X. Chen, X. Du, B. Guan, Y. Liu, H. Zhang, EGF enhances the migration of cancer cells by up-regulation of TRPM7, Cell Calcium 50 (2011) 559–568.
[52] K. Burridge, M. Chrzanowska-Wodnicka, Focal adhesions, contractility, and signaling, Annu. Rev. Cell Dev. Biol. 12 (1996) 463–518.
[53] R. Schneggenburger, E. Neher, Presynaptic calcium and control of vesicle fusion, Curr. Opin. Neurobiol. 15 (2005) 266–274.
[54] C.A. Reid, J.M. Bekkers, J.D. Clements, N- and P/Q-type Ca^{2+} channels mediate transmitter release with a similar cooperativity at rat hippocampal autapses, J. Neurosci. 18 (1998) 2849–2855.
[55] C.A. Reid, J.M. Bekkers, J.D. Clements, Presynaptic Ca^{2+} channels: a functional patchwork, Trends Neurosci. 26 (2003) 683–687.
[56] J. Qian, J.L. Noebels, Presynaptic Ca^{2+} channels and neurotransmitter release at the terminal of a mouse cortical neuron, J. Neurosci. 21 (2001) 3721–3728.
[57] P. Rybarczyk, M. Gautier, F. Hague, I. Dhennin-Duthille, D. Chatelain, J. Kerr-Conte, F. Pattou, J.M. Regimbeau, H. Sevestre, H. Ouadid-Ahidouch, Transient receptor potential melastatin-related 7 channel is overexpressed in human pancreatic ductal adenocarcinomas and regulates human pancreatic cancer cell migration, Int. J. Cancer 131 (2012) E851–E861.
[58] Y. Calle, N.O. Carragher, A.J. Thrasher, G.E. Jones, Inhibition of calpain stabilises podosomes and impairs dendritic cell motility, J. Cell Sci. 119 (2006) 2375–2385.
[59] M.S. Samuel, J.I. Lopez, E.J. McGhee, D.R. Croft, D. Strachan, P. Timpson, J. Munro, E. Schroder, J. Zhou, V.G. Brunton, et al., Actomyosin-mediated cellular tension drives increased tissue stiffness and beta-catenin activation to induce epidermal hyperplasia and tumor growth, Cancer Cell 19 (2011) 776–791.
[60] M.J. Paszek, N. Zahir, K.R. Johnson, J.N. Lakins, G.I. Rozenberg, A. Gefen, C.A. Reinhart-King, S.S. Margulies, M. Dembo, D. Boettiger, et al., Tensional homeostasis and the malignant phenotype, Cancer Cell 8 (2005) 241–254.
[61] I. Dhennin-Duthille, M. Gautier, M. Faouzi, A. Guilbert, M. Brevet, D. Vaudry, A. Ahidouch, H. Sevestre, H. Ouadid-Ahidouch, High expression of transient receptor potential channels in human breast cancer epithelial cells and tissues: correlation with pathological parameters, Cell Physiol. Biochem. 28 (2011) 813–822.
[62] M.X. Zhu, Multiple roles of calmodulin and other Ca(2+)-binding proteins in the functional regulation of TRP channels, Pflugers Arch. 451 (2005) 105–115.
[63] D.E. Clapham, Calcium signaling, Cell 131 (2007) 1047–1058.
[64] F. Haeseleer, Y. Imanishi, I. Sokal, S. Filipek, K. Palczewski, Calcium-binding proteins: intracellular sensors from the calmodulin superfamily, Biochem. Biophys. Res. Commun. 290 (2002) 615–623.
[65] A. Miyauchi, K.A. Hruska, E.M. Greenfield, R. Duncan, J. Alvarez, R. Barattolo, S. Colucci, A. Zambonin-Zallone, S.L. Teitelbaum, A. Teti, Osteoclast cytosolic calcium, regulated by voltage-gated calcium channels and extracellular calcium, controls podosome assembly and bone resorption, J. Cell Biol. 111 (1990) 2543–2552.
[66] K. Clark, J. Middelbeek, E. Lasonder, N.G. Dulyaninova, N.A. Morrice, A.G. Ryazanov, A.R. Bresnick, C.G. Figdor, F.N. van Leeuwen, TRPM7 regulates myosin IIA filament stability and protein localization by heavy chain phosphorylation, J. Mol. Biol. 378 (2008) 790–803.

Please cite this article in press as: D. Visser, et al., TRPM7 triggers Ca^{2+} sparks and invadosome formation in neuroblastoma cells, Cell Calcium (2013), http://dx.doi.org/10.1016/j.ceca.2013.09.003